



Process of magnetite fabric development during granite deformation

Manish A. Mamtani ^{a,*}, Sandra Piazolo ^{b,c}, Reinhard O. Greiling ^d, Agnes Kontny ^d, František Hrouda ^{e,f}

^a Department of Geology & Geophysics, Indian Institute of Technology, Kharagpur 721302, India

^b Department of Geological Sciences, Stockholm University, Stockholm, Sweden

^c Department of Earth and Planetary Sciences, GEMOC ARC Key National Centre, Macquarie University, 2109 NSW, Australia

^d Lehrstuhl für Strukturgeologie und Tektonophysik, Institut für Angewandte Geowissenschaften, Karlsruhe Institute of Technology, Hertzstrasse 16, 76187 Karlsruhe, Germany

^e Institute of Petrology and Structural Geology, Charles University, Albertov 6, CZ-128 43 Prague, Czech Republic

^f AGICO Inc., Ječná 29a, Box 90, CZ-621 00 Brno, Czech Republic

ARTICLE INFO

Article history:

Received 6 December 2010

Received in revised form 14 May 2011

Accepted 19 May 2011

Available online 12 June 2011

Editor: Y. Ricard

Keywords:

magnetite
fabric
deformation
granite
anisotropy of anhysteretic remanence
magnetization
electron back scattered diffraction

ABSTRACT

This study evaluates the fabric defined by magnetite grains in a syntectonically deformed granite and deciphers the processes that led to magnetite fabric development. Anisotropy of anhysteretic remanence magnetization (AARM) analysis is performed in samples taken from different parts of the granite to establish that the magnetite grains define a fabric. Along with microstructural studies, the AARM data help conclude that this fabric is on account of shape preferred orientation (SPO) of the magnetite grains. The intensity of magnetite fabric (degree of anisotropy of the AARM ellipsoid) is higher in the southern parts as compared to the north, which is inferred to indicate a strain gradient. Electron back scattered diffraction (EBSD) analyses of magnetite grains were performed to determine if there are intracrystalline deformation features that could have influenced magnetite shape and SPO, and thus AARM data. Detailed crystallographic orientation data coupled with orientation contrast imaging did not reveal any subgrains and/or significant variations in crystallographic orientations within magnetite grains. Instead, grains exhibit fractures and are in places associated with quartz pressure fringes. Hence, neither the SPO nor the variation in the magnetite fabric intensity in the granite can be attributed to intracrystalline deformation of magnetite by dislocation creep. It is concluded that the magnetite grains were rheologically rigid and there was relative movement between the magnetite and the matrix minerals (quartz, feldspar and biotite). These matrix minerals actually define the fabric attractor and the magnetite grains passively rotated to align with it. Thus it is demonstrated that the magnetite fabric in the granite stems from rigid body movement rather than dislocation creep.

© 2011 Elsevier B.V. All rights reserved.

1. Introduction

Research on granites in the past few decades has revealed that although many of them lack clear mesoscopic evidence of a deformation fabric, this can be recognized by performing anisotropy of magnetic susceptibility (AMS) studies (e.g., Bouchez, 1997; Tarling and Hrouda, 1993). As a consequence, an integration of field, microstructural and AMS data has helped infer the time-relationship between fabric development and tectonic deformation in several granites (e.g. Archanjo et al., 1995; Greiling and Verma, 2001; Majumder and Mamtani, 2009a; Rochette et al., 1994; Žák et al., 2009). Many granites are magnetite bearing and AMS on its own does not analyze fabric defined by only the magnetite grains in the rock. This is because all the mineral phases present in the rock irrespective of being diamagnetic (e.g. quartz), paramagnetic (e.g. biotite) or ferromagnetic *sensu lato*/ferrimagnetic (e.g. magnetite) contribute to its AMS. Thus, whilst AMS provides information about the bulk fabric

in the rock that can be linked to deformation, it does not indicate whether the magnetite grains also develop a fabric due to the same deformation. The fabric defined by magnetite can be determined by performing anisotropy of magnetic remanence (AMR) analysis (e.g., Jackson, 1991; McCabe et al., 1985; Petitgirard et al., 2009; Raposo and Gastal, 2009; Raposo et al., 2007; Trindade et al., 1999). AMR essentially stems from the shape anisotropy of ferrimagnetic magnetite (e.g. Tarling and Hrouda, 1993). Commonly used methods to determine AMR in rocks are measurement of IRM (isothermal remanence magnetization) and ARM (anhysteretic remanence magnetization) (e.g., Jackson, 1991). However, these methods do not provide any insight about the process/mechanism of magnetite fabric development. During fabric development, minerals can undergo rigid body rotation and/or recrystallization and may accommodate intracrystalline deformation by dislocation creep. With regards to magnetite, theoretical/experimental data (deformation mechanism map) indicate that at temperatures (T) > 600 °C it may undergo plastic deformation by dislocation creep (Ferré et al., 2003; Housen et al., 1995). Owing to its cubic crystallography and opaque nature, optical microscopy cannot help in recognizing intracrystalline plastic deformation features such as substructures i.e. systematic crystal bending

* Corresponding author at: Tel.: +91 3222 283388; fax: +91 3222 255303/282700.
E-mail address: mamtani@gg.iitkgp.ernet.in (M.A. Mamtani).

and subgrain boundaries within magnetite grains. However, such crystallographic features can be recognized by EBSD (electron back scattered diffraction) analysis (e.g., Agar and Lloyd, 1997; Boyle et al., 1998; Menegon et al., 2011; Piazolo et al., 2004; Prior et al., 2000; Storey and Prior, 2005). Thus, to quantify magnetite fabric and identify the processes that led to its formation AMR, microstructural, and EBSD data need to be integrated. Such an integrated approach has been adopted in this study with an aim to address the following questions.

- (a) Does high temperature deformation of magnetite embedded in a deforming granite matrix lead to development of subgrains and/or other evidences of intracrystalline deformation and dynamic recrystallization?
- (b) To what extent does such deformation influence the shape as well as shape preferred orientation (SPO) of magnetite in granite, which, in turn, is expected to influence the fabric intensity of magnetite petrofabric in the rock?

We address these questions by studying samples from the syntectonically deformed, Grenvillian age (955 ± 20 Ma; Gopalan et al., 1979) Godhra Granite located in the southern parts of the Aravalli Mountain Belt (northwest India; Fig. 1). This granite is taken as an example because it is ideal for a study focusing on the processes responsible for magnetite fabric development since it has been shown (Mamtani and Greiling, 2005, 2010; Sen, 2006; Sen and Mamtni, 2006; Sen et al., 2005) that (a) the emplacement and fabric development in the granite is syntectonic (b) intensity of AMS fabric as well as lineation varies from low in the north to high in the south, which is linked to the proximity of the southern part to the Central Indian Tectonic zone (c) high to low temperature deformation fabrics have been observed, where high-T fabrics such as chessboard pattern in quartz ($>650^\circ\text{C}$), although present throughout the granite, are dominant in the north, while medium-T (recrystallized feldspars; $450\text{--}600^\circ\text{C}$) and lower-T fabrics such as deformation twins in feldspars ($400\text{--}500^\circ\text{C}$) and kinked biotites ($\leq 300^\circ\text{C}$) dominate the southern part (Fig. 1c), (d) many samples of the granite are magnetite-bearing and have high mean magnetic susceptibility

($>500 \times 10^{-6}$ SI units) (e) magnetite occurs in association with ilmenite indicating that the magnetite formed at $T > 600^\circ\text{C}$ (Ghiorso and Sack, 1991; Haggerty, 1991). In this study the magnetite fabric (and its variation in the granite) is evaluated from petrographic and anisotropy of anhysteretic remanence magnetization (AARM) analysis. Subsequently, EBSD analysis is performed to evaluate the possible role of intracrystalline deformation in the fabric development of magnetite.

2. Magnetite fabric analysis

2.1. Petrography—grain size and aspect ratio data

The granite is dominantly coarse grained to porphyritic and a mesoscopic foliation is generally absent. Therefore, in earlier studies the fabric of the granite was identified from AMS analysis (Mamtani and Greiling, 2005; Sen and Mamtni, 2006; Sen et al., 2005). AMS gives orientation of three principal axes K_1 , K_2 and K_3 ($K_1 > K_2 > K_3$) of the AMS ellipsoid and the K_1K_2 plane represents the planar fabric (magnetic foliation) of the rock. For petrographic investigations, thin sections were prepared parallel to this magnetic foliation plane. Observations under transmitted light reveal that quartz, feldspar and biotite are the major mineral phases present. Opaque minerals comprise the minor phase, and ore petrography was performed on several polished thin sections from the northern and southern parts of the Godhra Granite. Samples were stained brown with ferrofluid for accurate identification of magnetite. Ferrofluid is a stable colloidal suspension of magnetite particles that range in size from 11 to 20 nm in a liquid medium (e.g. Kletetschka and Kontny, 2005). Magnetite grains, which are larger than a few micrometers have magnetic domains that generate large magnetic gradients above the polished surface and attract the particles of the ferrofluid. Hence, magnetite is stained brown with the ferrofluid and this allows its quick and clear distinction from other opaque phases under an optical microscope. Using this method, 6 different samples from different parts of the Godhra Granite were studied in detail. Altogether the grain size d (equal area diameter) and aspect ratio R (long/short axis ratio) of 225

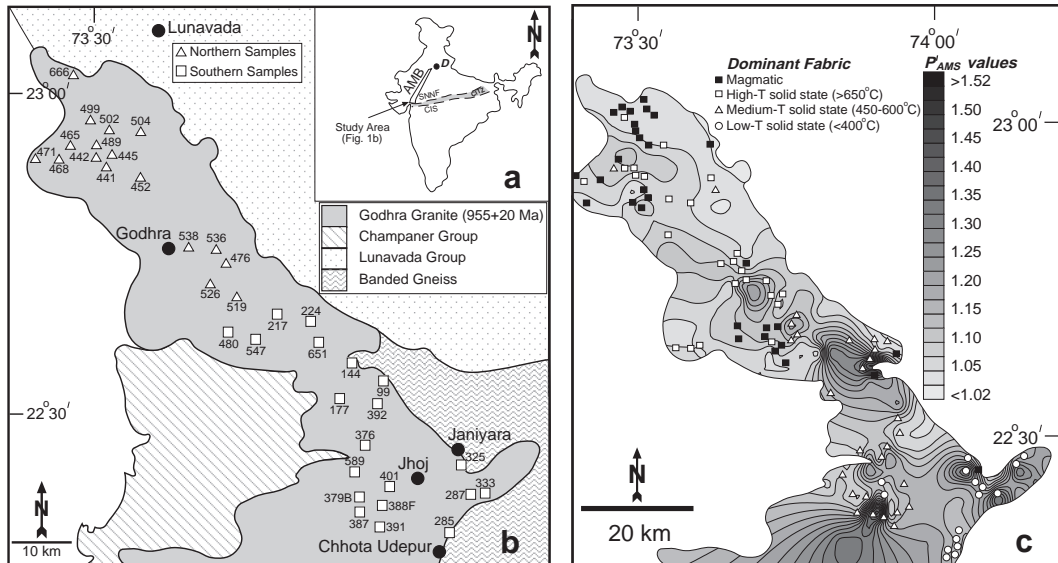


Fig. 1. (a) Map of India showing the Aravalli Mountain Belt (AMB) that lies to the north of the Central Indian Tectonic Zone (CITZ). The latter formed due to accretion of the northern and southern Indian shields during Palaeoproterozoic times (Yedekar et al., 1990). SNFF and CIS are the Son-Narmada-North Fault and Central Indian Suture that demarcate the northern and southern margins of the CITZ, respectively. (b) Geological map of the study area around the Godhra Granite. Locations of sampling sites in the north (triangles) and south (squares) on which anisotropy of anhysteretic remanence magnetization (AARM) analyses were made are shown. (c) Degree of anisotropy of magnetic susceptibility (P_{AMS}) map of the Godhra Granite. Dominant fabrics identified in different parts of the granite based on petrographic study are also shown along with the temperature range of the various high-T solid-state fabrics (after Sen, 2006).

magnetite grains were measured using digital image analysis. It was found that the granite is dominated by coarse magnetite grains mainly $\geq 75 \mu\text{m}$ (Fig. 2b), and the maximum size recorded is 852 μm (sample 388F). The magnetite grains have a shape anisotropy and their long dimensions (i.e., longest shape axis) are aligned sub-parallel to the longest shape axis of biotite, feldspar and quartz grains around them (Fig. 2c,d). Magnetite grains in the Godhra Granite have a measurable shape anisotropy (Fig. 2e), where the minimum aspect ratio R is 1.09 (sample 217), the maximum is 4.47 (sample 388F); the mean is 1.56.

2.2. AARM data

To obtain 3-dimensional information about the magnetite fabric, AARM analyses were performed on cylindrical granite cores (25.4 mm diameter \times 22 mm height) by applying a weak direct current (DC) field in the presence of a strong alternating current (AC) field (e.g., Aubourg and Robion, 2002; Hirt et al., 1995; Jackson et al., 1989; McCabe et al., 1985; Petitgirard et al., 2009; Raposo and Gastal, 2009;

Sagnotti et al., 1998; Trindade et al., 1999 etc.). It is known that populations of magnetite grains with distinctly different sizes (coarse and fine) may have different orientations, thus defining sub-fabrics. Since magnetite grain size and coercivity have an inverse relation (Day et al., 1977; Jackson et al., 1989) such sub-fabrics can be recognized through partial AARM (pAARM) analysis, where measurements are made over different coercivity windows e.g., 0–50 mT for grain size 100–500 μm and 50–90 mT for fine magnetite grains of 1–5 μm (e.g., Trindade et al., 1999). In the present study (a) magnetite grain size is dominantly coarse and there is no bimodal grain size distribution (Fig. 2a,b), (b) the alternating field (AF) demagnetization of the granite samples (Fig. 2f) showed very rapid and continuous decrease of the remnant magnetization with demagnetizing field. The median destructive field, which is the field that is necessary to remove half of the NRM, is 4 mT, and after demagnetization in a field of 30 mT, the remnant magnetization is less than 5% of the original value. In addition, the curve decreases smoothly and monotonously indicating a unimodal population of very low coercivity (coarse) magnetite

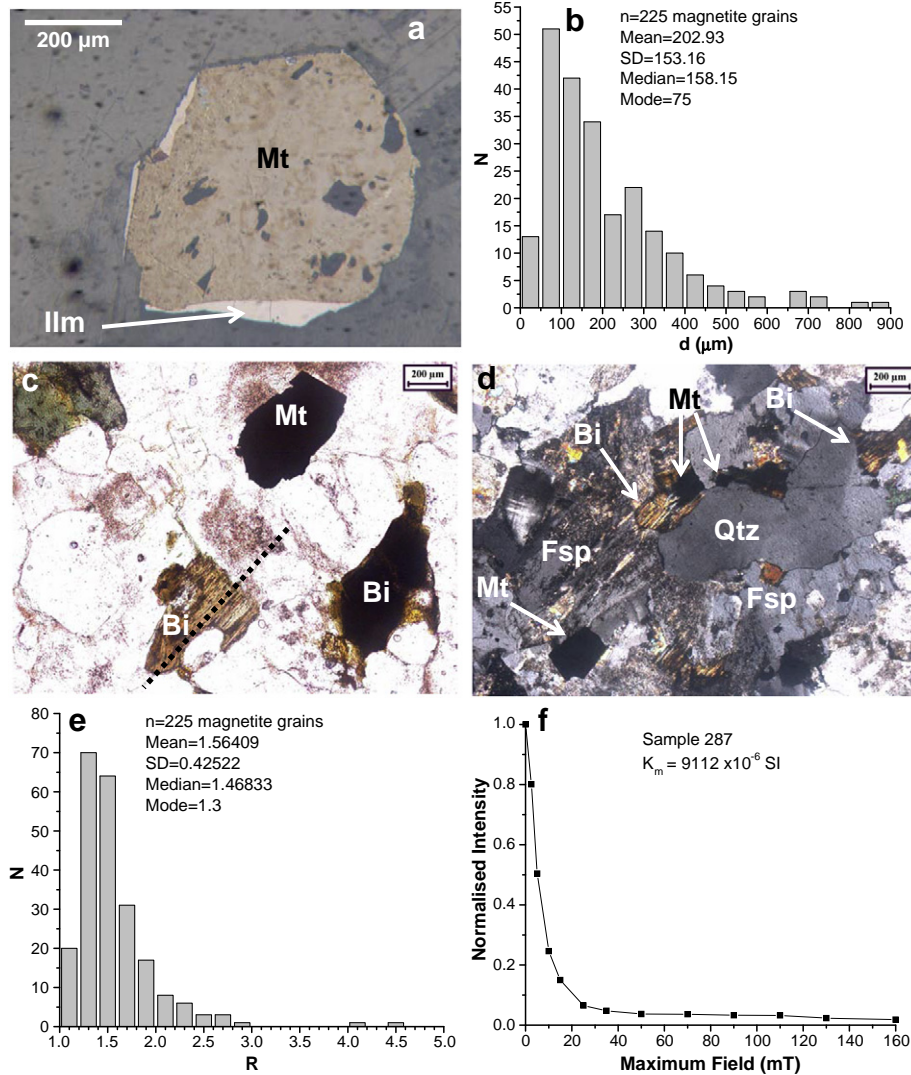
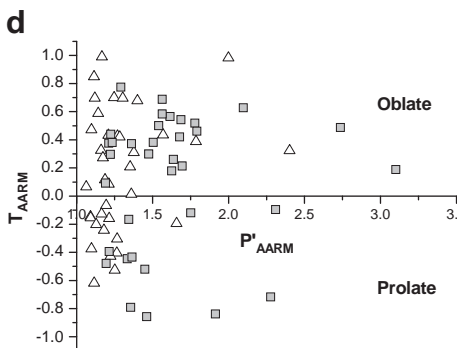


Fig. 2. (a) Photomicrograph of magnetite (Mt) grain (sample 388F) coexisting with ilmenite (Ilm). The thin section was stained with a ferrofluid. The latter stains only the magnetite grains and thus enables quick identification. (b) Histogram of grain size (d) of magnetite in 6 samples from different parts of the Godhra Granite. (c) and (d) are photomicrographs of thin sections taken in plane polarized light (sample 532) and crossed nicols (sample 217), respectively, highlighting the anisometric shapes of magnetite in the Godhra Granite. Note that the long axis (elongation direction) of the magnetite grain shapes is aligned sub-parallel with the elongated grains of biotite (Bi) and the magnetite elongation is parallel to this. (e) Histogram of aspect ratio (R) of magnetite in 6 samples from the granite indicating that the grains have shape anisotropy. (f) Representative AF demagnetization plot of a Godhra Granite sample. Complete demagnetization was achieved indicating low coercivity, which implies presence of coarse magnetite grains. SD = standard deviation in (b) and (e).

grains. Therefore, pAARM was not analyzed here, and anhysteretic magnetization was imparted with a DC field of $50 \mu\text{T}$ in the presence of an AC field of 80 mT using the AMU-1A Magnetizer (AGICO, Czech Republic). Appendix-A gives the technical details of the full procedure that was followed for AARM analysis.

AARM analysis was performed on 72 cores from 37 sites (Fig. 1b). Of these, 37 cores are from the northern and 35 from the southern sites. AARM analysis of each core yields the three principal axes of the AARM ellipsoid (A_1, A_2, A_3 , where $A_1 \geq A_2 \geq A_3$). A_1 defines the orientation of the magnetic lineation defined by the ferrimagnetic phase (in this case magnetite), while A_3 is the pole to the magnetic foliation (A_1A_2 plane). The data are used to calculate (a) the corrected degree of AARM anisotropy (P'_{AARM}), which quantifies eccentricity of the AARM ellipsoid, and (b) the shape parameter (T_{AARM}) (Jelínek, 1981; 1993); for oblate shapes $T_{\text{AARM}} > 1$ and $T_{\text{AARM}} < 1$ for prolate shapes (see Appendix-A for details of the methodology as well as formulae).



P'_{AARM} values of cores vary between 1.063 and 3.101 (Fig. 3a, Table 1). This implies that the samples have an eccentric AARM ellipsoid. Fig. 2c, d, and e shows that the magnetite grains in the granite have a grain shape anisotropy. The P'_{AARM} values obtained not only support this but also indicate that the 3-dimensional shape of magnetite grains is also anisotropic. In addition, P'_{AARM} values (Fig. 3a,b,c) are higher in the southern sites (mean $P'_{\text{AARM}} = 1.6$) than the northern sites (mean $P'_{\text{AARM}} = 1.3$). This is also noted in the P'_{AARM} vs. T_{AARM} plot (Fig. 3d).

Fig. 4a and b shows lower hemisphere equal area projections of the orientations of A_1 (lineation) and A_3 (pole to the foliation defined by A_1A_2 plane) respectively. For the Godhra Granite extensive AMS data exist (Mamtani and Greiling, 2005; Sen, 2006; Sen and Mamtani, 2006; Sen et al., 2005). For comparison, AMS data of the same cores that were subjected to AARM analyses are listed in Table 1. Like AARM, the AMS data are also represented by an ellipsoid with three principal axes K_1, K_2 and K_3 ($K_1 > K_2 > K_3$). Fig. 4c and d is the respective lower

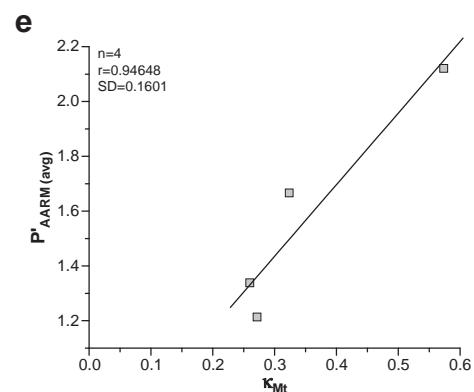
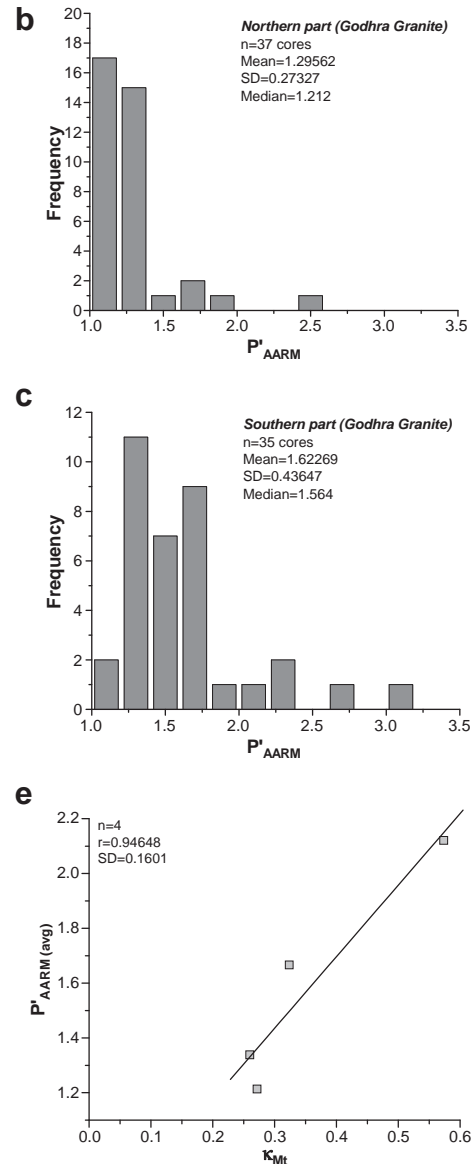


Fig. 3. (a) Map showing average degree of AARM ($P'_{\text{AARM}, \text{avg}}$) for the 37 sites investigated in this study. (b) and (c) are histograms of P'_{AARM} values obtained for individual cores from the northern and southern samples, respectively. Note the higher P'_{AARM} values in the southern samples as compared to the northern ones. (d) P'_{AARM} vs. T_{AARM} plot for the northern (triangles) and southern (squares) samples of the Godhra Granite. (e) Average degree of AARM ($P'_{\text{AARM}, \text{avg}}$) vs. strength of magnetite shape preferred orientation (K_{Mt}) plot for 4 samples of the Godhra Granite. The correlation coefficient (r) and standard deviation (SD) are mentioned on the plot.

Table 1

Anisotropy of anhysteretic remanence magnetization (AARM) data from the Godhra Granite, southern parts of Aravalli Mountain Belt (NW, India). AMS data (after Sen, 2006) for the same samples are also tabulated. A_m and K_m refer to mean remanence magnetization and susceptibility respectively. P'_{AARM} and P'_{AMS} refer to degree of anisotropy of the AARM and AMS ellipsoids respectively. T_{AARM} and T_{AMS} refer to the shape of the AARM and AMS ellipsoids respectively. A_1 and K_1 are the declination/inclination (D/I) of the maximum principal axis of the AARM and AMS ellipsoids respectively. A_3 and K_3 are the D/I of the minimum principal axis AARM and AMS ellipsoids respectively.

Sample	Azi/Dip	A_m (10^{-3})	P'_{AARM}	T_{AARM}	A_1 [D/I]	A_3 [D/I]	K_m (10^{-6})	P'_{AMS}	T_{AMS}	K_1 [D/I]	K_3 [D/I]
<i>Northern part (Godhra Granite)</i>											
441-1	35/80	34.95	1.187	0.117	238/61	48/29	5267	1.029	0.27	239/52	12/28
441/2	35/80	57.49	1.098	0.472	160/26	35/50	5266	1.031	-0.135	238/38	25/47
442/1	175/17	57.25	1.063	0.066	75/75	343/1	3739	1.022	0.409	87/62	353/2
442/3	175/17	58.87	1.091	-0.146	258/20	158/26	3931	1.024	-0.558	76/6	167/1
445/1	260/13	54.09	1.115	0.849	242/72	149/1	5014	1.036	0.634	261/54	155/12
445/2	260/13	50.66	1.194	-0.066	74/49	188/20	4906	1.055	-0.253	84/38	192/22
452-1	237/8	29.48	1.265	-0.405	106/15	209/39	5394	1.066	-0.488	105/11	214/58
452/2	237/8	54.18	1.251	-0.526	297/2	206/14	5275	1.06	-0.575	111/6	214/65
452/3	237/8	35.29	1.098	-0.375	108/14	18/2	4400	1.042	-0.687	97/13	358/34
465/1	300/52	12.03	1.161	0.326	311/73	151/16	951.6	1.091	0.16	303/62	157/24
465/2	300/52	12.49	1.352	0.208	264/32	354/1	808.9	1.11	0.335	278/36	179/12
465/3	300/52	7.238	1.212	0.085	62/11	154/6	482.6	1.043	0.331	241/42	151/0
468-1	172/25	26.79	1.247	0.700	298/52	180/20	4022	1.059	0.861	305/48	172/32
468/3	172/25	42.35	1.180	-0.243	260/26	168/3	4261	1.048	0.049	250/13	151/35
471/2	40/45	75.74	1.142	0.589	325/52	147/38	6534	1.045	0.431	302/47	145/40
471/1	40/45	77.19	1.120	0.696	275/35	132/49	6804	1.067	0.77	343/21	118/61
476/2	242/6	63.80	1.658	-0.194	174/64	6/25	9110	1.124	0.601	254/42	6/22
476/1	242/6	129.5	1.209	0.432	198/66	2/24	4665	1.211	0.137	196/71	345/17
489/2	182/5	37.09	1.092	-0.154	213/7	316/60	4703	1.043	-0.493	70/5	339/17
489/3	182/5	31.07	1.116	-0.619	251/2	154/71	3802	1.045	-0.471	251/5	154/58
499/1	20/5	58.76	1.269	0.428	265/16	357/7	6074	1.105	0.427	261/5	352/7
499/2	20/5	54.54	1.377	0.310	255/32	356/16	6309	1.119	0.453	256/17	349/10
499/3	20/5	64.55	1.283	0.420	249/19	340/4	7249	1.122	0.518	251/20	343/3
502-1	30/20	45.37	1.215	-0.159	276/30	113/59	6152	1.064	0.196	268/21	156/44
504/3	220/80	42.95	1.129	-0.202	278/20	187/2	4430	1.077	-0.242	274/11	178/24
519/c1	150/5	55.68	1.786	0.388	310/23	205/31	8123	1.262	0.529	303/19	204/27
519/c2	150/5	55.60	1.569	0.435	293/16	192/32	8265	1.208	0.292	292/15	194/29
526-1	240/0	7.594	2.402	0.323	308/27	57/33	654.7	1.102	0.483	348/56	207/28
526/2	240/0	19.14	1.165	-0.127	338/15	70/7	774.1	1.113	0.037	201/30	90/32
526/4	240/0	32.52	1.267	-0.305	103/45	341/28	1126	1.094	-0.25	124/47	334/39
536/2	185/20	10.05	1.999	0.982	73/49	276/39	2131	1.041	-0.008	230/19	136/12
536/3	185/20	23.92	1.360	0.013	104/42	358/16	2165	1.122	0.211	94/26	353/22
536/4	185/20	18.90	1.223	-0.427	279/39	168/23	2094	1.054	-0.498	265/41	359/5
538/1	215/20	150.3	1.400	0.678	217/55	38/35	9527	1.148	0.835	254/46	31/35
538/2	215/20	156.8	1.303	0.697	246/62	355/10	9551	1.14	0.899	92/35	0/3
666-1	170/60	10.80	1.173	0.273	133/59	334/30	1355	1.086	0.791	81/44	344/7
666/2	170/60	17.10	1.167	0.990	256/8	346/2	1600	1.078	0.748	79/32	339/15
<i>Southern Part (Godhra Granite)</i>											
99/1	15/55	198.6	2.310	-0.096	281/62	176/8	14413.09	1.415	-0.113	307/61	198/11
144/3	70/48	70.93	2.736	0.488	315/51	189/26	5474.75	1.263	0.350	298/51	159/31
144/1	70/48	108	1.505	0.382	282/39	165/29	4055.42	1.2	0.16	286/40	164/32
177/3	225/90	11.83	1.778	0.519	269/18	176/10	4090.13	1.192	-0.228	275/69	182/1
217-1	172/82	80.11	1.695	0.214	335/67	152/23	10432.47	1.264	0.324	349/63	155/26
217/3	172/82	83.23	1.637	0.261	350/66	138/20	10332.47	1.305	0.353	344/62	141/27
217/4	172/82	105.7	1.564	0.688	328/65	150/25	9930.47	1.253	0.393	339/62	158/28
224/3	320/30	458.7	1.752	-0.119	289/27	172/42	23982.46	1.268	-0.038	287/27	172/40
285/1	340/48	38.73	1.291	0.774	357/65	211/21	2090	1.118	0.877	332/53	201/26
285-3	340/48	26.84	1.190	0.093	334/52	118/33	2223	1.081	0.481	53/11	155/47
287/1	40/20	175.0	2.277	-0.717	330/31	239/1	9995	1.414	-0.702	325/31	63/12
325-X.1	85/14	241.9	1.914	-0.838	49/60	295/13	15.400	1.416	-0.681	56/61	324/1
379/b1	45/0	25.53	1.211	0.376	78/38	312/37	3250	1.136	0.293	75/22	308/56
379/b2	45/0	23.98	1.615	0.566	156/57	324/32	2658	1.286	0.355	132/55	324/34
333-1.2	190/20	44.98	1.356	-0.791	88/31	266/59	18.140	1.314	0.043	48/80	188/7
376/2	350/0	8.71	1.222	0.297	125/29	221/12	798.9	1.217	0.316	88/12	181/16
387/2	45/12	21.39	1.449	-0.520	267/41	166/12	2185	1.195	-0.578	268/43	145/30
387/3	45/12	25.56	1.234	0.381	290/63	177/11	2145	1.094	-0.045	280/47	177/12
388/f1	110/20	63.19	1.343	-0.166	274/29	16/20	5400	1.276	-0.516	280/28	14/7
388/f2	110/20	24.66	1.334	-0.446	114/8	19/30	2602	1.138	0.115	130/14	30/36
391/b1	128/18	13.30	1.540	0.501	245/37	144/15	2673	1.322	0.803	334/74	158/16
391/b2	128/18	23.27	1.564	0.584	246/13	152/19	2856	1.395	0.598	62/8	153/6
391/b3	128/18	16.12	1.687	0.543	222/68	315/1	2593	1.341	0.545	62/79	154/00
392-1	195/0	37.48	1.626	0.179	8/64	188/26	4994	1.208	0.45	18/65	186/25
392/2	195/0	50.25	1.475	0.299	338/69	174/20	4776	1.188	0.512	358/67	169/23
401-1	185/0	71	3.101	0.188	237/23	129/37	8844	1.493	0.02	252/30	134/38
401/2	185/0	18.82	1.678	0.420	269/13	168/39	2753	1.268	0.201	278/19	174/36
480-T	220/10	79.02	1.365	-0.433	322/45	124/43	4552	1.145	-0.756	324/41	103/41
480-T2	220/10	93.95	1.194	-0.479	321/52	87/25	5551	1.087	0.181	337/52	118/32
547/1	155/10	124.1	1.361	0.372	301/37	165/43	8408	1.163	0.509	292/32	168/42

(continued on next page)

Table 1 (continued)

Sample	Azi/Dip	A_m (10^{-3})	P'_{AARM}	T_{AARM}	A_1 [D/I]	A_3 [D/I]	K_m (10^{-6})	P'_{AMS}	T_{AMS}	K_1 [D/I]	K_3 [D/I]
<i>Southern Part (Godhra Granite)</i>											
547/2	155/10	92.05	1.225	0.439	324/28	194/50	6242	1.087	0.627	291/2	199/46
547/3	155/10	89.06	1.215	-0.394	294/37	156/45	6194	1.104	-0.083	295/34	147/51
589/3	275/8	176.5	1.461	-0.857	292/63	124/26	9433	1.298	0.02	277/71	154/10
651-b2	235/25	133.5	1.792	0.461	258/50	126/29	12,270	1.287	0.257	263/52	126/30
651-b3	235/25	145.6	2.097	0.628	255/53	124/27	14,820	1.39	0.402	257/48	130/28

hemisphere equal area projection of K_1 (lineation) and K_3 (pole to foliation defined by K_1K_2 plane) from the same samples shown in Fig. 4a and b. There is a similarity in the orientation of the principal directions of remanence (AARM) as well as susceptibility (AMS) ellipsoids. Fig. 4e and f is the lower hemisphere equal area projection of K_1 and K_3 data from all those samples of the Godhra Granite that have a mean susceptibility (K_m) below 500×10^{-6} SI units (Sen, 2006). Susceptibility and its anisotropy are to a large extent controlled by paramagnetic minerals (mainly biotite; e.g. Bouchez, 1997; Hrouda, 2002, 2010) in these granite samples. It is noted that orientations of K_1 and K_3 of those weakly magnetic granites (Fig. 4e,f) are similar to the K_1 and K_3 orientations of the other, strongly magnetic granites (Fig. 4c, d), as well as to the A_1 and A_3 orientations of the latter (Fig. 4a,b).

Fig. 5a and b shows the correlation between the shape factor T_{AARM} and T_{AMS} parameters for the northern and southern samples of the Godhra granite, respectively. The correlation coefficients, $r = 0.75$ and $r = 0.71$, respectively, indicate significant correlation. We performed

reduced major axis linear fitting on these data, which gives the relationship $T_{AARM} = 0.95T_{AMS}$ and $T_{AARM} = 1.25T_{AMS}$ for the northern and southern samples respectively. This good correlation implies that the AARM and AMS ellipsoids have similar shapes. Fig. 5c and d shows the correlation between the P_{AARM} and P_{AMS} parameters also for the northern and southern parts of the Godhra Granite, respectively. It may be noted that the P_{AARM} parameter is used for correlation studies instead of P'_{AARM} because of its very simple form (see Appendix-A for formulae). The correlation coefficients, $r = 0.40$ and $r = 0.77$, respectively, for the northern and southern samples, indicate intermediate to good correlation. The intermediate correlation coefficient in the northern part is related to a stronger scattering of the data. A least squares fitting straight line passing through the origin gives the relationships $\ln P_{AARM} = 2.66 \ln P_{AMS}$ and $\ln P_{AARM} = 2.08 \ln P_{AMS}$ for the northern and southern samples of the Godhra granite, respectively. Although the above correlation between AARM and AMS is different from that demonstrated by Jelínek (1993) for the case of

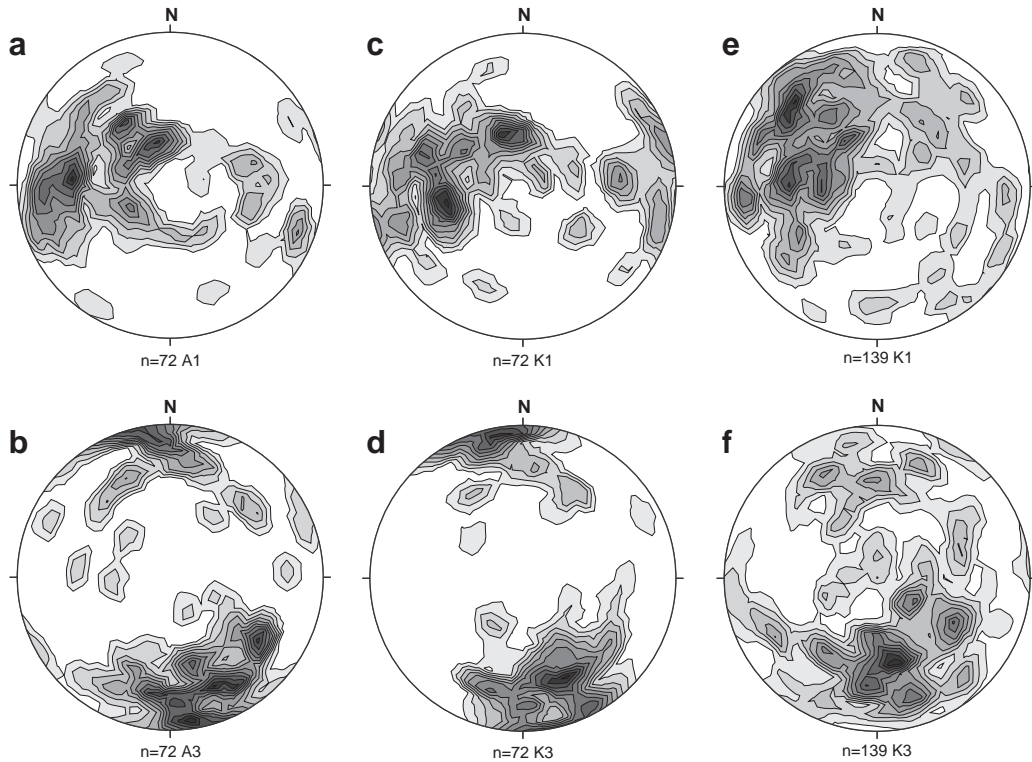


Fig. 4. Lower hemisphere equal area projections of orientations of A_1 (maximum principal axis of the AARM ellipsoid), A_3 (minimum principal axis of the AARM ellipsoid), K_1 (maximum principal axis of the AMS ellipsoid) and K_3 (minimum principal axis of the AMS ellipsoid). (a) and (b) are contoured A_1 and A_3 orientations, respectively, of the 72 cores of the strongly magnetic granites ($K_m > 500 \times 10^{-6}$ SI) analyzed in this study. (c) and (d) are the contoured K_1 and K_3 orientations, respectively, for the same cores. (e) and (f) are contoured K_1 and K_3 orientations, respectively, of 139 weakly magnetic granite samples ($K_m < 500 \times 10^{-6}$ SI) of the Godhra Granite. Note the similarity in orientations of A_1 and K_1 as well as A_3 and K_3 . See text for discussion. AMS data are after Mamtani and Greiling (2005), Sen et al. (2005) and Sen and Mamtani (2006). It may be noted that all contours are multiples of random distribution. Maximum density in (a) is 7.29 (at 273/36) with contours at 0.70, 1.40 unto 7.00. In (b) maximum density = 5.99 (at 171/6) with contours at 0.50, 1.00 unto 5.50. In (c) maximum density = 6.84 (at 257/48) with contours at 0.60, 1.20 unto 6.60. In (d) maximum density = 6.83 (at 156/30) with contours at 0.60, 1.20 unto 6.60. In (e) maximum density = 6.84 (at 315/24) with contours at 0.50, 1.00 unto 5.00. In (f) maximum density = 5.79 (at 165/42) with contours at 0.50, 1.00 unto 5.50.

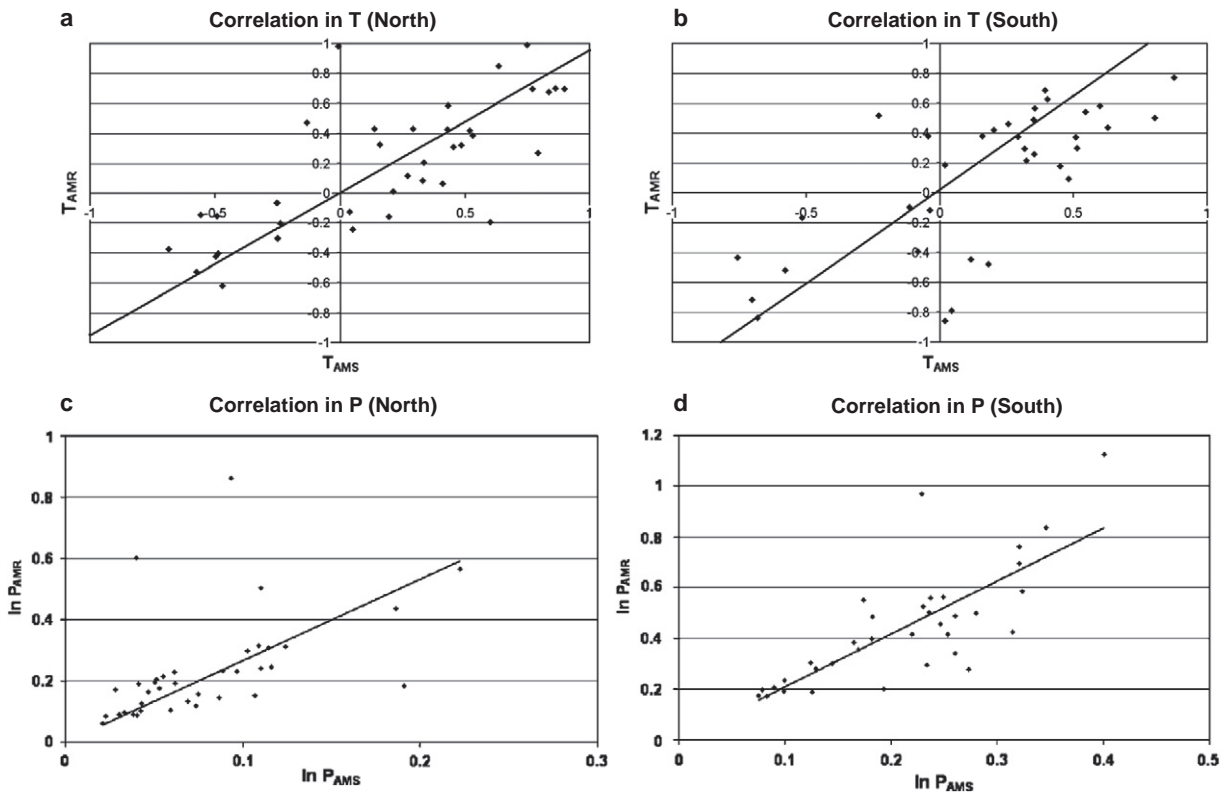


Fig. 5. Correlation between anisotropy of magnetic susceptibility (AMS) and anisotropy of magnetic remanence (AMR) data for the northern and southern samples. (a) and (b) show correlation between T_{AMS} and T_{AMR} for the northern and southern samples, respectively. (c) and (d) show the correlation between $\ln P_{AMS}$ and $\ln P_{AMR}$ for the northern and southern samples respectively.

Rayleigh region isothermal AMR ($\ln P_{AMR} = 3 \ln P_{AMS}$), nevertheless, it exists.

All the above data reveal that shapes of the AARM and AMS ellipsoids are similar and intensity of magnetite fabric is stronger towards the south in the Godhra Granite. This implies that in the granite the magnetite grains have a SPO that is parallel to the paramagnetic and diamagnetic phases (e.g. biotite, feldspar and quartz).

2.3. Shape preferred orientation (SPO) of magnetite from digital image analysis

To supplement information obtained about magnetite fabric from AARM analysis, we measured the shape preferred orientation (SPO) of magnetite grains in rock thin sections by performing digital image analysis. In this study we used the method proposed by Piazolo and Passchier (2002) to measure the intensity of SPO (strength of lineation) by determining the concentration parameter κ (strength of lineation) by determining the concentration parameter κ in foliation parallel sections (also see Masuda et al., 1999). In the past this method has provided useful SPO information in the granite being investigated (Sen and Mamtani, 2006), and good correlations between κ and magnetic fabric intensity have been established (also see Majumder and Mamtani, 2009b). Magnetite SPO (κ_{Mt}) is calculated here using this method on thin sections from 4 samples (468, 217, 144 and 388F; see Fig. 1 for locations); each section was prepared parallel to the K_1K_2 (magnetic foliation) plane (see Appendix-B for detailed methodology followed for this measurement). The κ_{Mt} value in each sample is >0.2 (Table 2). According to Piazolo and Passchier (2002) $\kappa > 0.2$ represents a significant SPO. The average P'_{AARM} values for the same samples are also listed in Table 2 and P'_{AARM} vs. κ_{Mt} plot is presented in Fig. 3e. The correlation between the two parameters is very high (0.95). Therefore, it is concluded that the AARM fabric in the Godhra Granite is on account of preferential alignment of anisometric magnetite grains.

3. EBSD analysis and orientation contrast imaging

To evaluate the processes and mechanisms that led to development of the magnetite fabric, EBSD analysis was performed. The Godhra Granite preserves evidence of having undergone solid state deformation at high-T (675–725 °C, quartz chessboard pattern thermometry; Mamtni and Greiling, 2010) to low temperature deformation (<400 °C) and magnetite-ilmenite association was present at T>600 °C (Ghiorso and Sack, 1991; Haggerty, 1991). According to the study of Housen et al. (1995) on anorthosite and Ferré et al. (2003) on migmatites, magnetite deforms by dislocation creep at T>600 °C. In light of the above, it is important to establish whether (a) magnetite grains embedded in granite accommodated intracrystalline deformation by dislocation creep? (b) plastic deformation (if any) of magnetite played a significant role in controlling variation in the intensity of magnetite fabric (P'_{AARM}) in different parts of the granite? Petrographic methods cannot provide information about intracrystalline deformation textures in opaque phases such as magnetite. EBSD analysis and orientation contrast imaging are

Table 2

Magnetite shape preferred orientation (SPO) data from the Godhra Granite calculated from digital image analysis using a petrographic microscope. The magnetite SPO is determined by measuring the concentration parameter (κ_{Mt}) using the Excel Worksheet of Piazolo and Passchier (2002). n = the number of magnetite grains from each sample. $P'_{AARM\ (avg)}$ = average P'_{AARM} value calculated from P'_{AARM} values of multiple cores of each sample (listed in Table 1). See Fig. 3e for correlation between κ_{Mt} and $P'_{AARM\ (avg)}$.

Sample	n	κ_{Mt}	$P'_{AARM\ (avg)}$
468	42	0.27	1.2135
217	41	0.32	1.666
144	42	0.57	2.1205
388F	43	0.26	1.3385

useful techniques for identifying intracrystalline deformation in minerals and characterizing the mechanisms of deformation in detail (e.g., Lloyd et al., 1997; Prior et al., 1999). Hence it was used to study the magnetite grains in the Godhra Granite. The reader is referred to Appendix-C for details of the analytical procedure and orientation contrast imaging procedure.

Two representative samples were investigated in detail, one from the north (sample 468) and one from the south (sample 388F); both represent cuts parallel to the magnetic foliation (K_1K_2) plane. OC imaging revealed that quartz and ilmenite exhibit strong, systematic crystallographic variations within single grains; both subgrains and gradual crystal bending are common (Fig. 6b), which are observed as variations in gray scale. In contrast, none of the magnetite grains

studied show subgrains or crystal bending in OC images (Fig. 6b). Two representative magnetite grains in each section were analyzed in detail using EBSD analysis, which confirm OC image results. None of the analyzed magnetite showed any significant and/or systematic intracrystalline deformation features such as continuous bending of the lattice or distinct subgrains (Fig. 6c,d). The crystal lattice is internally largely undeformed. Transects across grains show orientation variation below 1° (Fig. 6e). These variations are close to the angular resolution of 0.3° of the instrument and are not systematic (Fig. 6e,f) and they cannot be attributed to intracrystalline deformation and subgrain formation within magnetite grains. Observed misorientation changes $>1^\circ$ are abrupt and always directly associated with brittle fractures. For example, the crystallographic orientation

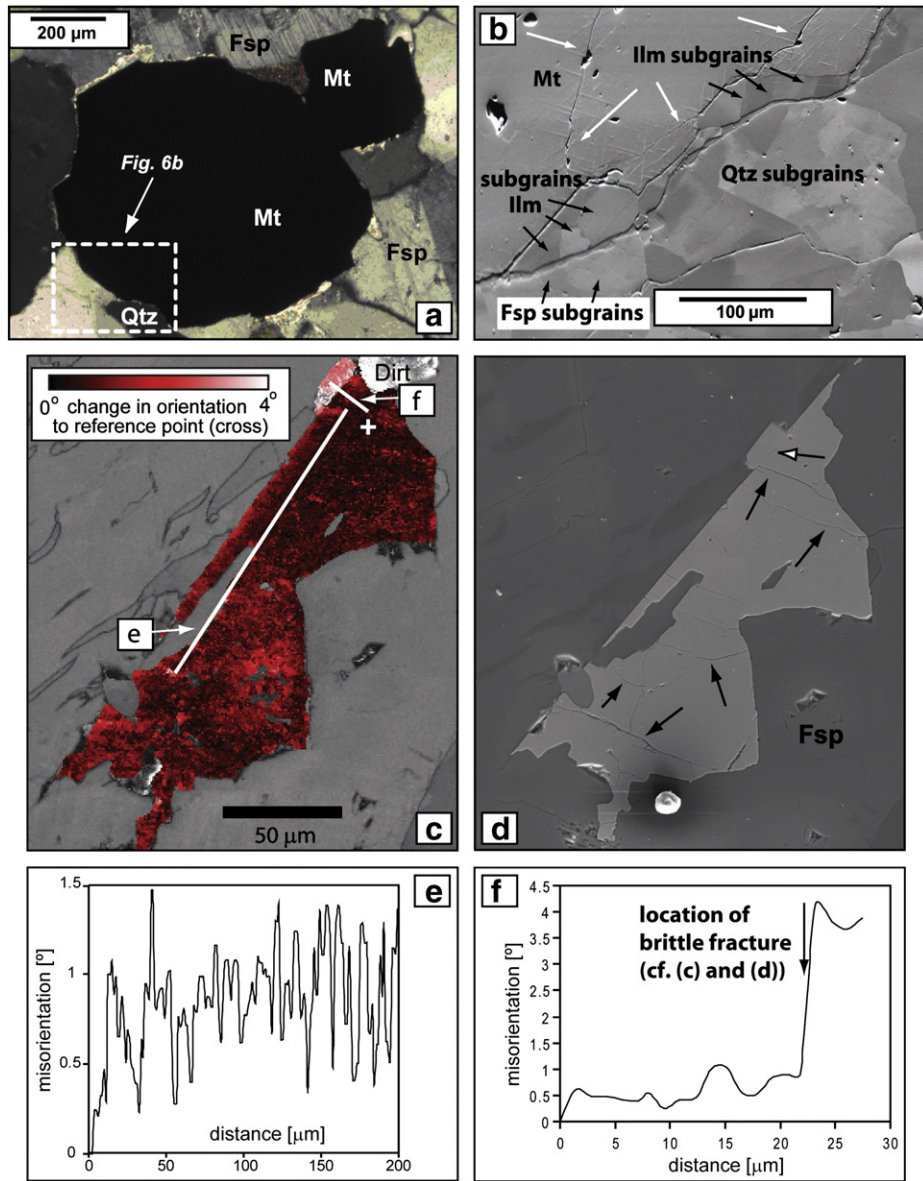


Fig. 6. (a) Photomicrograph of a magnetite (Mt) that was analyzed under SEM-EBSD (sample 388F). (b) Representative orientation contrast (OC) image of magnetite and phases around it (area is shown by a dashed box in Fig. 6a). Note the absence of any orientation contrast in the magnetite indicating absence of intracrystalline deformation. In contrast quartz (Qtz), feldspar (Fsp) and ilmenite (Ilm) adjacent to the magnetite show development of subgrains (black arrows) and gradual bending of the crystal lattice. Note the presence of brittle cracks in magnetite (white arrows). The criss-cross lines in magnetite are due to martitization; sample 388F. (c) EBSD data-based texture component map with 4° maximum difference from the crystallographic orientation marked at the white cross. In most of the grain, variation in crystallographic orientation is minor. On the upper corner of the grain an area of significantly different crystallographic orientation is seen across a fracture, which is marked in (d) by white arrow. (d) Secondary electron (SE) image of the same grain, showing that the differently oriented grain part seen in (c) is surrounded by fractures. (e) and (f) respectively show results of misorientation analysis along traverses marked by long and short white lines in (c). Arrow in (f) marks the location of the brittle fracture (white arrow in 6 d) across which of crystallographic misorientation in magnetite is $>4^\circ$.

change of $>4^\circ$ noted in Fig. 6f (along the NW–SE traverse marked in Fig. 6c) is across a fracture. Secondary Electron (SE) images confirm the presence of fractures within the studied magnetite (Fig. 6d). Observed fractures occur in magnetite grains of all sizes. They are straight, crossing the whole grain, or concave (e.g. Figs. 6d, 7b,c,d). No systematic conjugate set(s) of fractures are observed. A high percentage of the fractures are restricted to magnetite grains and do not extend into surrounding matrix phases (Fig. 7c). The majority of fractures show very little or no offset in the plane of view (Figs. 6b,d and 7c). However, there are cases where relative movement is seen (Fig. 7b,c,e,f). Here, the space generated between the magnetite and the matrix is interpreted to have been generated by movement along the fracture with a relative rotation of $\sim 10^\circ$ (Fig. 7c). In general, quartz fringes adjacent to magnetite grains are common (Fig. 7e,f).

4. Discussion

4.1. Parallelism of AARM and AMS orientation data

Orientations of the principal axes of the AARM (Fig. 4 a,b) and AMS (Fig. 4c,d) ellipsoids for the magnetite-bearing (strongly magnetic) granite samples are similar. Further, these orientations of the strongly magnetic granites are also similar to those of the weakly magnetic granites (Fig. 4 e,f). Thus, the AARM and AMS tensors are coaxial. On the microscopic scale also, a parallelism between the basal planes of biotite and long shape of magnetite grains is recorded. All the above indicate that in the Godhra Granite the orientations of the magnetite grains and the paramagnetic minerals in the matrix are similar and that the alignment of the grains of different phases was influenced by

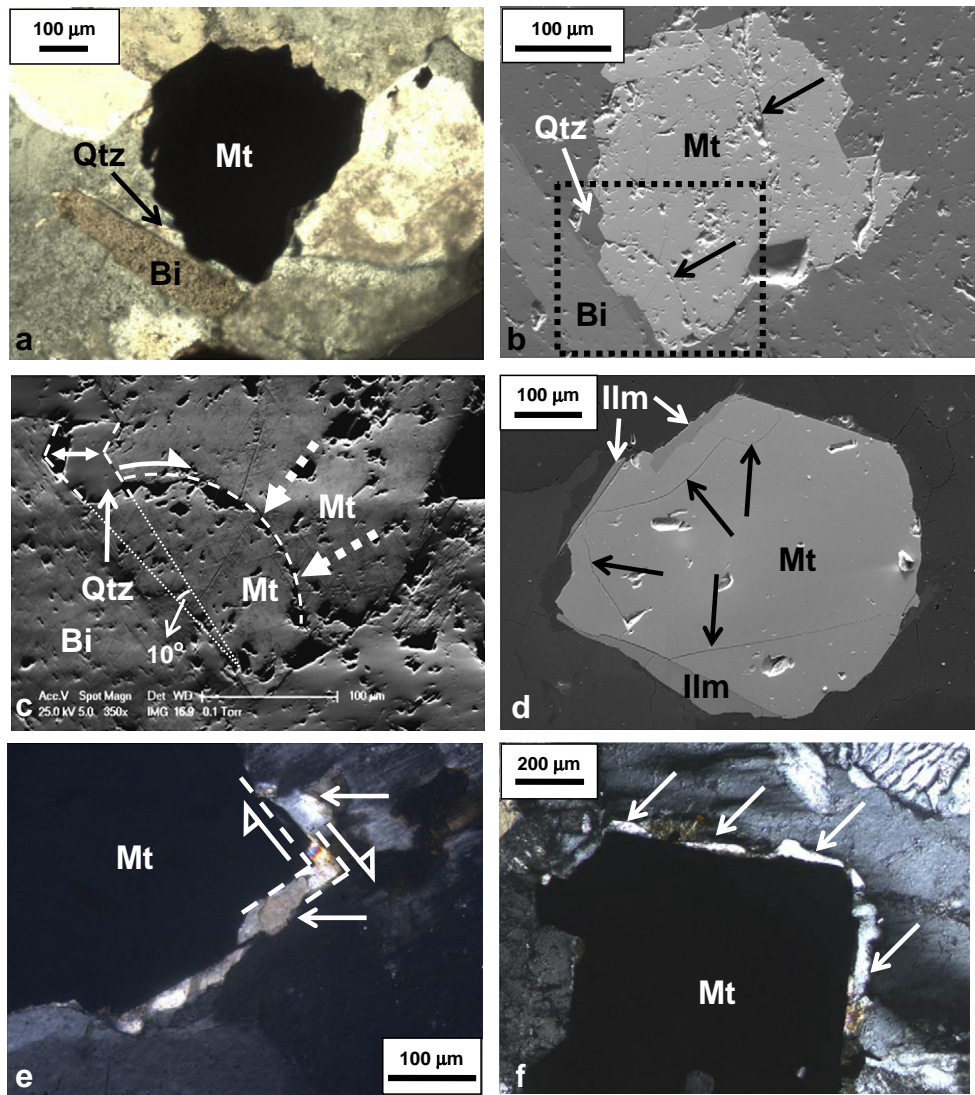


Fig. 7. Images and photomicrographs showing evidence of brittle deformation and rigid body movement of magnetite (Mt) grains in the Godhra Granite. (a) Photomicrograph of a magnetite grain (sample 468) set in a quartz-feldspathic-biotite matrix. Black arrow points to a thin fringe of quartz (Qtz) between the magnetite and biotite (Bi). (b) Secondary electron (SE) image of the magnetite shown in Fig. 7a. Black arrows point towards brittle cracks within magnetite. The dashed box demarcates the area shown in Fig. 7c. (c) Orientation contrast (OC) image (sample 468) showing presence of brittle cracks (white dashed arrows) within a magnetite as well as quartz filled pressure fringe next to the magnetite. The double-headed arrow near the top left margin shows the distance that the magnetite is inferred to have moved from adjacent biotite, and the space generated was filled by quartz. The dashed lines trace the outline of magnetite boundary on either side of the quartz fringe. The two lines show an angle of $\sim 10^\circ$ between them (angle between fine stippled lines), indicating a clockwise rotation of the magnetite grain relative to the biotite, with some of the rotation being accommodated by movement along the concave fracture (traced by bold dashed curved line). The criss-cross lines in the magnetite are due to martitization. (d) SE image showing brittle fractures (arrows) within magnetite grain in sample 388F; Ilm = ilmenite. (e) and (f) are photomicrographs showing presence of quartz pressure fringes (arrows) adjacent to magnetite grains (sample 388F). These imply that there was rigid body movement of magnetite grains relative to the matrix minerals and that there was loss of cohesion between the magnetite and the matrix; the locale of loss of cohesion was filled up by quartz fringes (see text for discussion). Half arrows on either side of the quartz fringe in (e) indicate the inferred anticlockwise movement of the magnetite relative to its matrix.

related fabric forming processes (e.g. Bascou et al., 2002; Raposo and Gastal, 2009; Raposo et al., 2003).

4.2. Variation in P' _{AARM} and its correlation with intensity of SPO

It is known that magnetite is crystallographically isotropic and hence any magnetic anisotropy associated with it is dominantly due to “shape anisotropy” (Tarling and Hrouda, 1993). However, some studies have advocated the possible role of “distribution anisotropy” (Hargraves et al., 1991), if there are clusters of several closely spaced magnetite grains (Cañón-Tapia, 2001; Grégoire et al., 1995). Such clusters are uncommon in the present samples (Fig. 2), which rules out any significant role of distribution anisotropy in controlling the magnetic anisotropy in the rocks. Microstructural information presented in this study (Fig. 2) demonstrates that the magnetite grains in the Godhra Granite have anisometric shapes and their long dimensions (long shape axis) tend to be aligned sub-parallel with those of the biotite and feldspar grains around them. This observation agrees well with the parallelism of AARM and AMS ellipsoid axes (Fig. 4). In this study, intensity of SPO defined by magnetite has been determined using (a) AARM measurement, which is a magnetic method and (b) measurement of the concentration parameter of magnetite (κ_{Mt}) from thin sections, which is a non-magnetic technique. Both analyses yield significant SPOs, where P' _{AARM} values are positive (Table 1) and κ_{Mt} values are >0.2 (Table 2). Moreover, the correlation coefficient (r) between P' _{AARM} and κ_{Mt} for the 4 samples for which data were generated using both the techniques is 0.95. This indicates that the correlation is strong and establishes that the intensity of magnetite SPO given by P' _{AARM} represents the SPO of magnetite grains.

Nevertheless, it should be noted that κ_{Mt} provides only direct information about SPO in two dimensions and is often based only on a few grains (~40 grains from serial thin sections of each sample studied here; Table 2). To obtain 3-dimensional SPO of magnetite from digital image analysis requires measurement of 2-dimensional SPO in three perpendicular planes, followed by integration of these data using other mathematical/statistical methods (e.g., Archanjo et al., 1995; Bascou et al., 2005; Launeau et al., 1990). However, for a statistically reliable data for a minor mineral phase like magnetite, such 2-dimensional measurements would have to be made on serial thin sections from each of the three perpendicular planes. In contrast, P' _{AARM} directly provides three dimensional information calculated from at least a few hundred magnetite grains in a single core and hence is much more accurate and time efficient. Thus, since P' _{AARM} and κ_{Mt} measured on the magnetic foliation K_1K_2 correlate, the three dimensional P' _{AARM} information can be used to infer the three dimensional SPO of magnetite.

4.3. Variation in P' _{AARM} and Strain

Based on AMS studies, the emplacement and fabric development in the Godhra Granite has been inferred to be syntectonic with Grenvillian age tectonic rejuvenation of the CITZ that lies to its south (Mamtani and Greiling, 2005). Moreover, the P' _{AMS}, intensity of magnetic lineation (L _{AMS}) as well as intensity of mineral lineation (SPO defined by biotite and feldspar) have been shown to be higher in the south as compared to the north. These variations have been attributed to higher strain in the south on account of its proximity to the CITZ (Sen and Mamtani, 2006; Sen et al., 2005). The present study reveals that the anisotropy of magnetic remanence (AMR) and AMS correlate well (Fig. 5). The AARM data also reveal that the southern samples have a stronger P' _{AARM} as compared to the north (Fig. 3). It is inferred that these data are indicative of a stronger magnetite SPO in the south. This provides further evidence that regional strain related to CITZ activity has influenced development of the magnetite fabric. Accordingly, the magnetite fabric in the southern part developed under greater strain. This also validates the statement of Dunlop and Özdemir (1997) that AMR may correlate directly with strain.

4.4. Deformation mechanism of magnetite in deforming granite

Experimental studies have revealed that magnetite can undergo intracrystalline deformation by dislocation creep (Hennig-Michaeli and Siemes, 1982; Müller and Siemes, 1972). Based on results from experimental data Atkinson (1977) produced a deformation mechanism map for magnetite at 662 °C (see references in Atkinson, 1977 for details). Subsequently, Housen et al. (1995) investigated magnetite grains (20–40 µm size) from the Parry Sound Shear Zone (Ontario) and concluded that magnetite undergoes ductile deformation by dislocation creep at 630 °C. Their deformation mechanism map was based on the constitutive equations given by Atkinson (1977). Ferré et al. (2003) used the deformation mechanism map of Housen et al. (1995) to indirectly infer dislocation creep in magnetite grains (20–200 µm size) from migmatites (deformation $T \leq 800$ °C) of Morton, Minnesota (Superior Province). They also stated that the main features of the deformation mechanism map given by Housen et al. (1995) remain valid between 600–800 °C. In contrast, EBSD analysis on magnetite and ilmenite in gabbroic shear zones (>900 °C–550 °C) revealed dislocation creep to be the dominant deformation mechanism in ilmenite, but not in magnetite (Agar and Lloyd, 1997). Likewise, crystallographic fabric analysis of mylonitic granulites from a shear zone in the Ribeira Belt (Brazil; Bascou et al., 2002) revealed a strong crystallographic preferred orientation (CPO) of titanohematite grains, which was inferred to be due to dislocation creep. However, no CPO was observed in the magnetite grains.

Our data show that there is no significant evidence for intracrystalline crystal-plastic deformation by dislocation creep such as presence of low angle boundaries and subgrains (Figs. 6 and 7) in magnetite grains of the investigated granite. This is true for small as well as large magnetite grains in the northern as well as southern samples. Variations in crystallographic orientations occur only across fractures (Fig. 6c–f). Thus, our SEM based analyses do not confirm dislocation creep as the dominant deformation mechanism of magnetite at $T > 600$ °C and grain size > 50 µm in the Godhra Granite. Rather, brittle deformation, i.e. fracturing, is observed. The timing of the fracturing is interpreted to be at still high temperatures, as in some “filled” fractures ilmenite is present. While the surrounding silicates (quartz, feldspar and biotite) deformed mainly by dislocation creep (cf. Fig. 6b), magnetite behaved rigidly and underwent brittle deformation. It is further envisaged that the behavior of magnetite continued to remain rigid as temperatures decreased, which is supported by the presence of quartz-filled pressure fringes (Fig. 7b,c,e,f).

4.5. Fabric forming process of magnetite in the granite and origin of AARM signature

EBSD analysis reveals that the magnetite in the granite is not plastically deformed and did not undergo intracrystalline deformation. Therefore, the anisometric shape of magnetite grains is not due to intracrystalline deformation of magnetite, but is on account of their initial growth during crystallization. As a consequence, whilst the high P' _{AARM} values in the southern samples are related to high regional strain and are indicative of a relatively strong magnetite SPO, this cannot be attributed to a dominance of intracrystalline deformation i.e. dislocation creep or climb within magnetite grains. This implies that there must be some other mechanism responsible for the SPO development of magnetite. Since the magnetite grains are fractured and the surrounding silicate minerals have developed subgrains, it is clear that magnetite was relatively rigid compared to the matrix minerals. Moreover, magnetite grains commonly have their long (shape) axis aligned sub-parallel with the elongated matrix minerals (e.g., Fig. 2c,d). The similarity between the orientations of the principal axes of the AARM and AMS ellipsoids (Fig. 4) also implies parallelism between fabric defined by magnetite and matrix minerals. Consequently, rigid body movement (and rotation) of magnetite is

the only feasible mechanism that could have led to the observed SPO development of magnetite. The Godhra Granite has been inferred to have emplaced under oblique simple shear (Mamtani and Greiling, 2005). We infer that during syntectonic emplacement and fabric development under oblique simple shear, the long (shape) axis of magnetite grains aligned with the fabric attractor (Passchier, 1997) defined by silicate minerals. While magnetite grains were rigid and accommodated strain by fracturing and rigid body rotation, the matrix minerals accommodated strain by intracrystalline deformation (cf. Fig. 6b). With progressive deformation and decrease in temperatures, there was a loss of cohesion between some of the magnetite grains and their neighboring lower viscosity phases (silicate minerals). These areas of loss of cohesion became the loci where fluids ponded and quartz was crystallized, thus forming the observed fringes around the magnetite grains (cf. Fig. 7b,e,f).

It has already been demonstrated by Sen and Mamtani (2006) that the southern part of the Godhra Granite has a stronger SPO that is defined by biotite and feldspar grains. As a consequence, the magnetite grains, which follow the fabric (attractor) defined by matrix minerals, also have a stronger SPO in the southern samples and this is the reason for the measured higher AARM intensity in the southern part of the Godhra Granite.

5. Conclusions

This study demonstrates that magnetite grains in the Godhra Granite define a fabric which can be quantified in three dimension from AARM analysis. Further, in the study area the intensity of the AARM fabric increases from north to the southern parts of the granite. From previous regional studies (Mamtani and Greiling, 2010; Sen and Mamtani, 2006; Sen et al., 2005) it is known that there is a strain gradient in the area. Thus AARM intensity can be used to identify the strain gradient in a study area. EBSD analysis of magnetite grains within thin sections of the rocks did not reveal changes in crystallographic orientations within single magnetite grains that can be linked to intracrystalline deformation due to dislocation creep or glide. Instead, magnetite grains commonly show fractures. Significant variations in crystallographic orientations (ca 4°) were noted only across fractures. As a consequence, the shape of magnetite grains in the granite cannot be attributed to intracrystalline deformation of magnetite by dislocation creep. Therefore, the variation in intensity of magnetite fabric cannot be caused by plastic deformation of magnetite.

During fabric development, magnetite was rheologically rigid relative to the matrix minerals (quartz, feldspar and biotite). These matrix minerals accommodated most of the strain by crystal plastic deformation and defined the fabric attractor into which the magnetite grains tended to align. This resulted in similar AARM and AMS ellipsoid orientations. It is therefore inferred that in the Godhra Granite, rigid body movement and rotation of magnetite relative to matrix minerals were the most important fabric forming processes.

The present study highlights the importance of integrating AARM data with results from EBSD studies of magnetite grains to evaluate the processes that led to fabric defined by magnetite. Although the example discussed is that of magnetite grains in granite from India, the approach adopted provides a direction for similar research to be performed on any deformed magnetite-bearing rock, in which deformation mechanisms and processes responsible for fabric development need to be evaluated.

Acknowledgements

The authors thank three anonymous reviewers and editor Yanick Ricard for detailed constructive reviews, which helped improve the manuscript significantly. MAM thanks the Alexander von Humboldt (AvH) Foundation (Germany) for the award of a Humboldt Research

Fellowship, to pursue a part of this research at the University of Heidelberg (Germany) from 2006 to 2007 as well as for the award of a Europe Research Fellowship to perform AARM analysis in Brno (Czech Republic). SEM-EBSD studies were done at Stockholm University (Sweden) in 2009 and MAM's visit was funded by the AvH Foundation under the "Resumption of Research Stay" Alumni programme for Humboldt Research Fellows. SP thanks the Swedish Research Council (VR 621-2004-5330), the Knut and Alice Wallenberg Foundation (financing of equipment) and the European Science Foundation (ESF) through their EUROCORES Programme Euro-MinSci, FP6 for financial support. The work of FH in this paper was partially supported financially by the Ministry of Education and Youth of the Czech Republic (Scientific Program MSM0021620855). Assistance provided by Taritwan Pal (IIT Kharagpur) in measuring SPO of magnetite is gratefully acknowledged.

Appendix A. Methodology of AARM measurement

AARM measurements were made on oriented cylindrical cores (25.4 mm diameter and 22 mm height). Each cylindrical specimen was initially demagnetized in a LDA-3A AF demagnetizer (AGICO, Czech Republic). Demagnetization was done in an AC field of 100 mT and during the process, the specimen was tumbling and rotating in the equipment. After the sample had been demagnetized, anhysteretic magnetization was imparted in one direction (position) with a DC field of 50 µT in the presence of an AC field of 80 mT using the AMU-1A Magnetizer (AGICO, Czech Republic). The above fields were considered suitable because AF demagnetization curve (Fig. 2f) revealed almost complete demagnetization at 30 mT field, which indicates only low coercivity coarse magnetite grains. Subsequently, remnant magnetization was measured using the Spinner Magnetometer JR6A (AGICO, Czech Republic). After the remanence measurement, the sample was once again tumble demagnetized in an AC field of 100 mT. Anhysteretic magnetization was imparted in another direction and the remanence was measured. Similarly, this procedure of demagnetization followed by imparting anhysteretic remanence and its measurement was repeated for 12 directions (6 parallel, and 6 antiparallel magnetization directions, which is part of magnetizing design-A of the AMU-1A magnetizer; this measurement scheme gives the most accurate results). The data were processed using the programme AREF (AGICO, Czech Republic), based on the theory by Jelínek (1993). The parameters obtained using the measurement are the orientations and magnitudes of the three principal axes of the AARM ellipsoid (A_1, A_2, A_3 , where $A_1 \geq A_2 \geq A_3$). These basic data are used to calculate the degree of AARM anisotropy (P_{AARM}), the corrected degree of AARM anisotropy (P'_{AARM}), and shape parameter (T_{AARM}), defined as follows (Jelínek, 1981)

$$P_{\text{AARM}} = A_1 / A_3 \quad (\text{A.1})$$

$$P'_{\text{AARM}} = P_{\text{AARM}}^{\alpha}, \alpha = \sqrt{(1 + T_{\text{AARM}}^2 / 3)} \quad (\text{A.2})$$

$$T_{\text{AARM}} = 2 \ln(A_2 / A_3) / \ln(A_1 / A_3) - 1 \quad (\text{A.3})$$

P_{AARM} and P'_{AARM} are measures of the eccentricity of the AARM ellipsoid. The P_{AARM} parameter is very simple and convenient in correlation studies between AARM and AMS, while the P'_{AARM} parameter is more complex, based on values of all three axes of the AARM ellipsoid. T_{AARM} parameter gives the shape (oblate or prolate) of the ellipsoid. If $T_{\text{AARM}} < 0$, the AARM ellipsoid is prolate. If $T_{\text{AARM}} > 0$, the ellipsoid is oblate. If $T_{\text{AARM}} = 0$, the ellipsoid is neutral.

Appendix B. Methodology of measuring SPO of magnetite grains from digital image analysis

Piazolo and Passchier (2002) proposed measurement of intensity of SPO (strength of lineation) by determining the concentration parameter κ in foliation parallel sections (also see Masuda et al., 1999). Here magnetite SPO (κ_{Mt}) is calculated using this method. Several frames (photomicrographs) of an oriented thin section were captured using a digital camera attached to the petrological microscope. Since the thin section was fitted within an XY object guide on the microscope stage an identical orientation was maintained while capturing various frames. In each frame, the opaque phases were first physically identified in reflected light to distinguish between magnetite and other opaque phases (e.g., ilmenite). Subsequently only the magnetite was mapped and binarized using Leica Qwin digital image analysis software. The angle (θ) between the X-axis of the microscope stage and long (shape) axis of the magnetite grains was measured automatically using the above software. The above procedure was followed for all the frames of a particular thin section. According to Piazolo and Passchier (2002) (a) at least 30 grains of a particular mineral are necessary to get a statistically reliable measure of the SPO (κ) defined by that mineral and (b) $\kappa > 0.2$ indicates a significant SPO. Since magnetite is not a major mineral in the granite, it was necessary to perform this analysis on multiple oriented thin sections from each sample. In the present study θ (angle) of >40 magnetite grains were calculated from each sample. These θ values were then processed using the Excel sheet of Piazolo and Passchier (2002) to calculate κ_{Mt} , which gives the strength of lineation defined by magnetite grains and is a measure of the intensity of magnetite SPO.

Appendix C. Procedure followed for EBSD analysis

Thin-sections investigated were chemically polished using colloidal silica before SEM based analyses that were conducted on a Philips XL-30-ESEM-FEG (Department of Geology and Geochemistry, Stockholm University, Sweden). EBSD patterns were collected on rectangular grids by moving the electron beam at a fixed step size (1, 2 or 3 μm). Complete crystallographic orientation data were obtained from EBSD patterns (e.g. Adams et al., 1993) using a 25 kV accelerating voltage, working distance of 15 to 20 mm in low vacuum mode (0.3 Torr). The patterns were automatically indexed using the CHANNEL 5 software from Oxford Instruments—HKL at an average of 80% indexed EBSD patterns. On all maps a correction was performed, which minimizes the change in measured orientation due to varying beam-sample-detector geometry to $<0.5^\circ$ per millimeter of scanned distance. Data processing included replacement of non-indexed solutions by the most common neighbor orientation. Furthermore, a filter was applied to remove single, isolated pixels of a very different orientation to their surrounding areas. The degree of processing required to fill non-indexed data points in this way, without introducing artifacts, was tested carefully and optimized accordingly (see e.g. Piazolo et al., 2006). In order to enhance detection of possible low angle boundaries (LABs), one pass of a 3×3 Kuwahara filter (an edge detection image analysis tool) were used (Kuwahara and Eihō, 1976). The angular resolution of crystallographic orientation data is in the order of 0.3° . Using the above described methodology, textural component maps were prepared. These show the difference in misorientation of each point analysis relative to a chosen reference orientation and allow accurate detection of crystallographic variations that could be related to intracrystalline deformation mechanisms. Orientation contrast (OC) imaging with the SEM allows different crystallographic orientations within a same grain to be seen as variations in gray scale. In the present study OC imaging was performed using two forescatter detectors situated at the lower part of the EBSD phosphorous screen (Prior et al.,

1996). OC images suggested the presence of fractures in many magnetite grains. To verify that features interpreted as cracks and fractures were truly such, secondary electron (SE) imaging was performed on the same samples, this time carbon coated at 20 kV acceleration voltage.

It may be noted that magnetite lattice preferred orientation (LPO) was not studied here because magnetite is crystallographically cubic and for a reliable LPO, two crystallographic axes in more than 100 magnetite grains need to be taken into account (Skemer et al., 2005). Since magnetite is a minor phase in the rock this was not possible. More importantly, magnetite grains studied here did not show intracrystalline deformation features (Section 3; Figs. 6, 7) and are hence not expected to show any LPO.

References

- Adams, B.L., Wright, S.I., Kunze, K., 1993. Orientation imaging: the emergence of a new microscopy. *Met. Transac.* 24A, 819–831.
- Agar, S.M., Lloyd, G.E., 1997. Deformation of Fe-Ti oxides in gabbroic shear zones from the MARK area. In: Karson, J.A., Cannat, M., Miller, D.J., Elthon, D. (Eds.), *Proceedings of the Ocean Drilling Program, Scientific Results*, 153: College Station, TX (Ocean Drilling Program), pp. 123–141.
- Archano, C.J., Launeau, P., Bouchez, J.L., 1995. Bulk magnetic fabric versus shape fabrics of magnetite and biotite in magnetite-bearing pluton (Gameleiras, Northeast Brazil). *Phys. Earth Planet. Inter.* 89, 63–75.
- Atkinson, B.K., 1977. The kinetics of ore deformation: its illustration and analysis by means of deformation-mechanism maps. *Geol. Förh.* 99, 186–197.
- Aubourg, C., Robion, P., 2002. Composite ferromagnetic fabrics (magnetite, greigite) measured by AMS and partial AARM in weakly strained sandstones from western Makran Iran. *Geophys. J. Int.* 151, 729–737.
- Bascou, J., Raposo, M.I.B., Vauchez, A., Egydio-Silva, M., 2002. Titanohematite lattice-preferred orientation and magnetic anisotropy in high-temperature mylonites. *Earth Planet. Sci. Lett.* 198, 77–92.
- Bascou, J., Camps, P., Dautria, J.M., 2005. Magnetic versus crystallographic fabrics in a basaltic lava flow. *J. Vol. Geoth. Res.* 145, 119–135.
- Bouchez, J.L., 1997. Granite is never isotropic: an introduction to AMS studies of granitic rocks. In: Bouchez, J.L., Hutton, D.W.H., Stephens, W.E. (Eds.), *Granite: From Segregation of Melt to Emplacement Fabrics*. Kluwer Academic Publishers, pp. 95–112.
- Boyle, A.P., Prior, D.J., Banham, M.H., Timms, N.E., 1998. Plastic deformation of metamorphic pyrite: new evidence from electron-backscatter diffraction and foreshatter orientation-contrast imaging. *Miner. Deposita* 34, 71–81.
- Cañón-Tapia, 2001. Factors affecting the relative importance of shape and distribution anisotropy in rocks: theory and experiments. *Tectonophysics* 340, 117–131.
- Day, R., Fuller, M., Schmidt, V.A., 1977. Hysteresis properties of titanomagnetites: grain-size and compositional dependence. *Phys. Earth Planet. Inter.* 13, 260–267.
- Dunlop, D.P., Özdemir, Ö., 1997. *Rock Magnetism: Fundamentals and Frontiers*. Cambridge University Press, Cambridge.
- Ferré, E., Teysier, C., Jackson, M., Thill, J.W., Rainey, E.S.G., 2003. Magnetic susceptibility anisotropy: a new petrofabric tool in migmatites. *J. Geophys. Res.* 108 (B2), 2086. doi:10.1029/2002JB001790.
- Ghiorso, M.S., Sack, R.O., 1991. Fe-Ti oxide geothermometry: thermodynamic formulation and the estimation of intensive variables in silicic magmas. *Contrib. Min. Petrol.* 108, 485–510.
- Gopalan, K., Trivedi, J.R., Merh, S.S., Patel, P.P., Patel, S.G., 1979. Rb-Sr age of Godhra and related granites, Gujarat (India). *Proc. Indian Acad. Sci. (Earth Planet. Sci.)* 88A, 7–17.
- Grégoire, V., de Saint Blanquat, M., Nedelec, A., Bouchez, J.L., 1995. Shape anisotropy versus magnetic interactions of magnetite grains: experiments and application to AMS in granitic rocks. *Geophys. Res. Lett.* 22, 2765–2768.
- Greiling, R.O., Verma, P.K., 2001. Strike-slip tectonics and granitoid emplacement: an AMS fabric study from the Odenwald Crystalline Complex, SW Germany. *Mineral. Petrol.* 72, 165–184.
- Haggerty, S.E., 1991. Oxide textures—a mini-atlas. In: Lindsley, D.H. (Ed.), *Oxide minerals: petrologic and magnetic significance*: Rev. Mineral., 25, pp. 129–220.
- Hargraves, R.B., Johnson, D., Chan, C.Y., 1991. Distribution anisotropy: the cause of AMS in igneous rocks? *Geophys. Res. Lett.* 18, 2193–2196.
- Hennig-Michaeli, C., Siemes, H., 1982. Compression experiments on natural magnetite crystals at 200 °C and 400 °C at 400 MPa confining pressure. In: Goodman, G.E., Heuze, F.E. (Eds.), *Issues in Rock Mechanics, Twenty-Third Symposium on Rock Mechanics*. American Institute of Mining, Metallurgical and Petroleum Engineers, New York, pp. 380–388.
- Hirt, A.M., Evans, K.F., Engleter, T., 1995. Correlation between magnetic anisotropy and fabric for Devonian shales on the Appalachian Plateau. *Tectonophysics* 247, 121–132.
- Housen, B.A., van der Pluijm, B.A., Essene, E.J., 1995. Plastic behaviour of magnetite and high strains obtained from magnetic fabrics in the Parry Sound shear zone, Ontario Grenville Province. *J. Struct. Geol.* 17, 265–278.
- Hrouda, F., 2002. The use of the anisotropy of magnetic remanence in the resolution of the anisotropy of magnetic susceptibility into its ferromagnetic and paramagnetic components. *Tectonophysics* 347, 269–281.
- Hrouda, F., 2010. Modelling relationship between bulk susceptibility and AMS in rocks consisting of two magnetic fractions represented by ferromagnetic and paramagnetic minerals—implications for understanding magnetic fabrics in deformed rocks. *J. Geol. Soc. India* 75, 254–266.

- Jackson, M., 1991. Anisotropy of magnetic remanence: a brief review of mineralogical sources, physical origins, and geological applications, and comparison with susceptibility anisotropy. *PAGEOPH* 136, 1–28.
- Jackson, M., Sprowl, D., Ellwood, B., 1989. Anisotropies of partial remanence and susceptibility in compacted black shales: grainsize and composition-dependent magnetic fabric. *Geophys. Res. Lett.* 16, 1063–1066.
- Jelínek, V., 1981. Characterization of magnetic fabric of rocks. *Tectonophysics* 79, T63–T67.
- Jelínek, V., 1993. Theory and measurement of the anisotropy of isothermal remanent magnetization of rocks. *Trav. Géophysiques* 37, 124–134.
- Kletetschka, G., Kontny, A., 2005. Identification of magnetic minerals by scanning electron microscope and application of ferrofluid. *Stud. Geophys. Geod.* 49, 153–162.
- Kuwahara, M., Eihō, S., 1976. Processing of radioisotope angiographic images. In: Preston, K., Onoe, M. (Eds.), *Digital Processing of Biomedical Images*. Plenum Press, New York, pp. 187–203.
- Launeau, P., Bouchez, J.L., Benn, K., 1990. Shape preferred orientation of object populations: automatic analysis of digitized images. *Tectonophysics* 180, 201–211.
- Lloyd, G.E., Farmer, A.B., Mainprice, D., 1997. Misorientation analysis and the formation and orientation of subgrain and grain boundaries. *Tectonophysics* 279, 55–78.
- Majumder, S., Mamtni, M.A., 2009a. Magnetic fabric in the Malanjkhanda Granite (Central India)—implications for regional tectonics and Proterozoic Suturing of the Indian Shield. *Phys. Earth Planet. Inter.* 172, 310–323.
- Majumder, S., Mamtni, M.A., 2009b. Intensity of shape preferred orientation in a granite and its tectonic implications. *Curr. Sci.* 96, 156–160.
- Mamtni, M.A., Greiling, R.O., 2005. Granite emplacement and its relation with regional deformation in the Aravalli Mountain Belt (India)—inferences from magnetic fabric. *J. Struct. Geol.* 27, 2008–2029.
- Mamtni, M.A., Greiling, R.O., 2010. Serrated quartz grain boundaries, temperature and strain rate: testing fractal techniques in a syntectonic granite. In: Spalla, I., Marotta, A.M., Goss, G. (Eds.), *Advances in Interpretation of Geological Processes: Refinement of Multi-Scale Data and Integration in Numerical Modelling*. Special Publications, 332. Geological Society, London, pp. 35–48.
- Masuda, T., Kugimiya, Y., Aoshima, I., Hara, Y., Ikei, H., 1999. A statistical approach to determination of mineral lineation. *J. Struct. Geol.* 21, 467–472.
- McCabe, C., Jackson, M.J., Ellwood, B.B., 1985. Magnetic anisotropy in the Trenton limestone: results of a new technique, anisotropy of anhysteretic susceptibility. *Geophys. Res. Lett.* 12, 333–336.
- Menegon, L., Piazolo, S., Pennacchioni, G., 2011. The effect of Dauphiné twinning on plastic strain in quartz. *Contrib. Mineral. Petrol.* 161, 635–652.
- Müller, P., Siemes, H., 1972. Zur Festigkeit und Gefügeregelung von experimentell verformten Magnetitzenzen (Strength and preferred orientation of experimentally deformed magnetite ores). *Neues Jahrb. Mineral. Abh.* 117, 39–60.
- Passchier, C.W., 1997. The fabric attractor. *J. Struct. Geol.* 19, 113–127.
- Petitgirard, S., Vauchez, A., Egydio-Silva, M., Bruguier, O., Camps, P., Monié, P., Babinski, M., Mondou, M., 2009. Conflicting structural and geochronological data from the Ibituruna quartz-syenite (SE Brazil): effect of protracted “hot” orogeny and slow cooling rate? *Tectonophysics* 477, 174–196.
- Piazolo, S., Passchier, C.W., 2002. Controls on lineation development in low to medium grade shear zones: a study from the Cap de Creus peninsula, NE Spain. *J. Struct. Geol.* 24, 25–44.
- Piazolo, S., Bestmann, M., Prior, D.J., Spiers, C.J., 2006. Temperature dependent grain boundary migration in deformed-then-annealed material: observations from experimentally deformed synthetic rocksalt. *Tectonophysics* 427, 55–71.
- Piazolo, S., Seward, G., Seaton, N., Prior, D.J., 2004. The potential of combined in-situ heating experiments and detailed EBSD analysis in the investigation of grain scale processes such as recrystallization and phase transformation. *Mate. Sci. Forum* 467–470, 1407–1412.
- Prior, D.J., Trimby, P.W., Weber, U.D., Dingley, D.J., 1996. Orientation contrast imaging of microstructures in rocks using forescatter detectors in the scanning electron microscope. *Mineral. Mag.* 60, 859–869.
- Prior, D.J., Wheeler, J., Brenker, F.E., Harte, B., Matthews, M., 2000. Crystal plasticity of natural garnet: new microstructural evidence. *Geology* 28, 1003–1006.
- Prior, D.J., Boyle, A.P., Brenker, F., Cheadle, M.C., Day, A., Lopez, G., Peruzzo, L., Potts, G.J., Reddy, S., Spiess, R., Timms, N.E., Trimby, P., Wheeler, J., Zetterström, L., 1999. The application of electron backscatter diffraction and orientation contrast imaging in the SEM to textural problems in rocks. *Am. Mineral.* 84, 1741–1759.
- Raposo, M.I.B., Gastal, M.C.P., 2009. Emplacement mechanism of the main granite pluton of the Lavras do Sul intrusive complex, South Brazil, determined by magnetic anisotropies. *Tectonophysics* 466, 18–31.
- Raposo, M.I.B., D’Agrella-Filho, M.S., Pinse, J.P.P., 2007. Magnetic fabrics and rock magnetism of Archaean and Proterozoic dike swarms in the Southern São Francisco craton, Brazil. *Tectonophysics* 443, 53–71.
- Raposo, M.I.B., D’Agrella-Filho, M.S., Siqueira, R., 2003. The effect of magnetic anisotropy on paleomagnetic directions in high-grade metamorphic rocks from the Juiz de Fora Complex, SE Brazil. *Earth Planet. Sci. Lett.* 209, 131–147.
- Rochette, P., Scaillet, B., Guillot, S., Lefort, P., Pecher, A., 1994. Magnetic properties of the high Himalayan leucogranites—structural implications. *Earth Planet. Sci. Lett.* 126, 217–234.
- Sagnotti, L., Speranza, F., Winkler, A., Mattei, M., Funiciello, R., 1998. Magnetic fabric of clay sediments from the external northern Apennines (Italy). *Phys. Earth Planet. Inter.* 105, 73–93.
- Skemer, P., Katayama, I., Jiang, Z., Karato, S-i., 2005. The misorientation index: development of a new method for calculating the strength of lattice-preferred orientation. *Tectonophysics* 411, 157–167.
- Sen, K., 2006. Analysis of deformation fabric in the Godhra Granite, Aravalli Mountain Belt (India): an integrated field microstructural and AMS investigation. Unpublished Ph.D. thesis, Indian Institute of Technology, Kharagpur (India), 153 pp.
- Sen, K., Mamtni, M.A., 2006. Magnetic fabric, shape preferred orientation and regional strain in granitic rocks. *J. Struct. Geol.* 28, 1870–1882.
- Sen, K., Majumder, S., Mamtni, M.A., 2005. Degree of magnetic anisotropy as a strain intensity gauge in ferromagnetic granites. *J. Geol. Soc. London* 162, 583–586.
- Storey, C.D., Prior, D.J., 2005. Plastic deformation and recrystallization of garnet: a mechanism to facilitate diffusion creep. *J. Petrol.* 46, 2593–2613.
- Tarling, D.H., Hrouda, F.H., 1993. *The Magnetic Anisotropy of Rocks*. Chapman & Hall, London.
- Trindade, R.I.F., Raposo, M.I.B., Ernesto, M., Siqueira, R., 1999. Magnetic susceptibility and partial anhysteretic remanence anisotropies in the magnetite-bearing granite pluton of Tourão, NE Brazil. *Tectonophysics* 314, 443–468.
- Yedekar, D.B., Jain, S.C., Nair, K.K.K., Dutta, K.K., 1990. The central Indian collision suture. *Geol. Surv. India, Sp. Publ.* 28, 1–43.
- Žák, J., Verner, K., Klominsky, J., Chlupáčová, M., 2009. “Granite tectonics” revisited: insights from comparison of K-feldspar shape-fabric, anisotropy of magnetic susceptibility (AMS), and brittle fractures in the Jizera granite Bohemian Massif. *Int. J. Earth Sci.* 98, 949–967.